atmosphere

MDPI

Article

Variations in the Peczely Macro-Synoptic Types (1881–2020) with Attention to Weather Extremes in the Pannonian Basin

János Mika [1,*], Csaba Károssy [2] and László Lakatos [1]

[1] Institute of Geography and Environmental Sciences, Eszterhazy Karoly Catholic University, Leanyka 6, 3300 Eger, Hungary; lakatos.laszlo@uni-eszterhazy.hu
[2] ELTE Savaria University Faculty, Karolyi Gaspar sq. 4, 9700 Szombathely, Hungary; c.karossy@gmail.com
* Correspondence: mika.janos@uni-eszterhazy.hu; Tel.: +36-70-330-79-50

Abstract: Daily Peczely circulation types are investigated over 140 years (1881–2020). After presenting monthly mean frequencies and durations of the 13 circulation types, two further questions are investigated: (i) How do the circulation types influence local weather extremes?; (ii) Are there significant trends in the frequency of the original and the grouped circulation types in the recent monotonically warming 50 year period (1971–2020)? The answers are as follows: (i) Four local weather extremes were investigated in nine grid-points of the Pannonian Basin and analyzed in the central months of the seasons. It was established that high precipitation and wind maxima occur in almost all circulation types and months, whereas for both high temperature maxima and low temperature minima, there are six circulation types, where no extremity occurred in one, two, or three investigated months. (ii) In the last 50 years, 37% of the linear seasonal frequency trends have been significant. However, these trends are rarely significant in the shorter monotonously warming (1911–1940) and cooling (1941–1970) 30-year periods. Therefore, the significant trends of the last 50 years are unlikely to be the direct consequences of the monotonous hemispherical warming. Since these hemispherical temperature trends are most likely caused by different sets of physical reasons, the reality of the presented circulation frequency trends needs to be validated by climate models.

Keywords: circulation type; Pannonian Basin; Peczely; cyclone; anticyclone; weather extreme; climate change

check for updates

Citation: Mika, J.; Károssy, C.; Lakatos, L. Variations in the Peczely Macro-Synoptic Types (1881–2020) with Attention to Weather Extremes in the Pannonian Basin. *Atmosphere* **2021**, *12*, 1071. https://doi.org/10.3390/atmos12081071

Academic Editor: Chuan Yao Lin

Received: 15 July 2021
Accepted: 16 August 2021
Published: 20 August 2021

Publisher's Note: MDPI stays neutral with regard to jurisdictional claims in published maps and institutional affiliations.

Copyright: © 2021 by the authors. Licensee MDPI, Basel, Switzerland. This article is an open access article distributed under the terms and conditions of the Creative Commons Attribution (CC BY) license (https://creativecommons.org/licenses/by/4.0/).

1. Introduction

Weather extremes are connected with large-scale circulation patterns, including the mesoscale objects embedded in them. The present paper deals with two main aspects of atmospheric circulation, as follows:

- the classification of weather maps into pre-defined discrete types of circulation;
- the impact of global warming on large-scale circulation.

Macro-synoptic (or macro-circulation) classification is based on spatial fields of sea level pressure or mid-tropospheric geopotential (e.g., [1–3] in case of the Peczely types). Since its first appearance in the literature, probably connected with the names of van Bebber and Köppen [4], macro-synoptic types often meet application in diagnostic and sometimes in prognostic tasks of descriptive or applied climatology, weather forecasting (e.g., [5–7]), and in air-pollution meteorology [8].

The description and catalogue of Hungary's macro-synoptic fields appeared in the work of Péczely [1]. This catalogue contains a daily classification of the sea-level pressure fields from 1877 until 1956. The next publication of the updated code series was issued 26 years later [2].

Peczely's classification has been widely used for diagnostic purposes (e.g., [9,10]) to understand connections between the circulation and local weather, sometimes including its variability, too. In air-pollution meteorology, where relatively short series of measurements

are often an obstacle to final conclusions, macro-synoptic types can be interfaces between the concentrations and local weather [11]. Since the early 1990s, further applications of the Peczely classification have been published [12–15].

Scope of this paper is focused on circulation changes, so basic statements on the reasons of climate change [16], or regional features of weather extremes [17] related to the ongoing climate change are not comprehended by this Section.

Recent research [18] makes it unequivocal that tropical areas have expanded poleward by 70–200 miles in both hemispheres during 1979–2009, also shifting the subtropical dry zones, mid-latitude jets, and storm tracks towards the poles. The mid-latitude circulation patterns are also perturbed in the Arctic areas observed in the recent past and simulated for the future [19]. In connection with these changes, the frequency of the persistent blocking anticyclones is likely changing at the adjacent temperate latitudes [20], or they concern particular regional non-linearity, such as the impact of warming on the rainfall in the Sahel [21] or the effect of soil moisture on diurnal maximum temperature [22]. The observed circulation changes in the tropics are also tackled by the papers [23–25].

A large amount of empirical evidence on changes of one or the other features of circulation are established, but in most cases there is little or no evidence of their attribution to climate change [26]. These empirical results are as follows.

Storm tracks over the North Atlantic–Europe sector moved northward as indicated by multi-proxy evidence over the North Atlantic [27–29]. Over Northern Hemisphere mid-latitudes, the summer zonal wind speeds have weakened in the mid-troposphere [30–32]. In boreal summer there have been increasing synoptic wavenumbers since the late 1970s [33].

Multiple reanalyses and radiosonde observations show an increasing number of extratropical cyclones over the Northern Hemisphere since the mid-20th century [34,35]. In recent decades, the number of deep cyclones (central pressure <980 hPa) in the Northern Hemisphere has decreased in both winter [36,37] and summer [38]. The blocking frequency has increased at lower latitudes over the Atlantic [34] and in the Greenland region in boreal summer [39].

There is weak evidence that stationary wave amplitude has increased over the North Atlantic region [40], possibly as a result of the weakening of the North Atlantic storm track and transfer of energy to the mean flow and stationary waves [37]. In boreal summer, Northern Hemisphere subtropical stationary waves show a robust amplification in modern reanalyses, which is coupled with significant regional changes in observed precipitation amounts [41].

Such a circulation response is, however, not necessarily consistent with the expected long-term response to global warming which rather suggests an overall weakening of stationary wave circulations [42], and it could represent a transient response to the Artic amplification observed in recent decades [43].

In general, atmospheric blocking can affect the water cycle and lead to negative precipitation anomalies in the region of the blocking anticyclone and positive anomalies in the surrounding areas [44]. In this way, blocking can also be associated with extreme events such as heavy precipitation [45] and drought [46].

Many climate models still underestimate the occurrence of blockings, at least in winter over the north-eastern Atlantic and Europe [47], which leads to caution in the interpretation of their results.

A summer increase of the number of cyclones over the Atlantic–European sector [48] is consistent with the increase in the number of very strong fronts over Europe. The authors of [49] showed that the number of very deep cyclones (<960 hPa) increased from 1979 to 1990 and then declined until 2010 in the North Atlantic while the number reached a peak in about 2000 and then decreased until 2010 over the North Pacific.

Empirical circulation classifications [50,51] and objective statistical methods [52,53] are used for European circulation classifications. The results of the two approaches are commonly combined and compared [54,55].

Both approaches make it possible to provide analyses of temporal changes [56,57]. In [56], long-term variations are established at multi-decadal time scales, but they are also different in the different seasons. At the same time, [57] finds in several global climate model experiments that no unequivocal changes can be established in Central Europe either in summer or in winter.

This result based on global climate models contradicts several other investigations that explain a more persistent flow over Europe, explaining this tendency with weakening of the temperature gradient, i.e., weakening of the tropospheric zonal flow, as a result of human-induced climate change [58–61].

The present paper is further structured as follows: Section 2 comprehends the analyzed circulation and local weather data including those that characterize the hemispherical warming during the last 50 years. Section 3 presents the statistical results in three sub-Sections starting with the primary results of synoptic climatology. The second part of the results represent the distribution of selected daily extreme values among the circulation types. Finally, in the third part of the results linear trends of the various circulation types are analyzed for the 1971–2020 period of hemispherical warming, compared to three other 30-year periods of the total 140 years of existence of the Peczely circulation types. The results are discussed in Section 4, followed by a short conclusion in Section 5 and the References.

2. Materials and Methods

The 13 macro-circulation types defined by Peczely [1,2] are listed in Table 1, in the original grouping, based on the typical wind direction. The coding takes place subjectively, but the 140-year archive of diurnal types (1881–2020) is the product of two experts, only. Until 1983, the author of the classification performed the coding, continued by his colleague, co-author of the present paper, C. Karossy.

Table 1. The 13 circulation types of the Peczely (1957) macro-synoptic classification [1], originally defined for Hungary (Hu). The original table by Peczely was edited in German, to characterize the 13 circulation types. The brief descriptions of each type were translated to English by one of the authors (JM).

Meridional Types	Zonal and Central Types
	Types Connected with Western Current:
Types Connected with Northern Current:	zC—zonal flow, slightly cyclonic influence
mCc—Hu is in the rear of a West-European cyclone	Aw—anticyclone extending from the west
AB—anticyclone over the British Isles	As—anticyclone to the south from Hungary
CMc—Hu is in the rear of a Mediterranean cyclone	**Types Connected with Eastern Current:**
	An—anticyclone to the north from Hungary
Types Connected with Southern Current:	AF—anticyclone over Fenno-Scandinavia
mCw—Hu is in the fore of a West-European cyclone	**Types of Pressure Centers:**
Ae—anticyclone to the east from Hungary	A—anticyclone center over Hungary
CMw—Hu is in the fore of a Mediterranean cyclone	C—cyclone center over Hungary

All methods and results involve this classification. Figure 1 presents examples of each circulation type, grouped according to the typical direction of the driving current, as presented above in Table 1.

The majority of the calculations apply to the Excel software package, except for the significance of the linear trends in Section 3.3, which applied Statistical Package for the Social Sciences (SPSS ver. 20).

In the first set of results (see in Section 3.1) univariate monthly statistics of average frequency and average duration is calculated for the most recent 1991–2020 period. These calculations follow the definition of relative frequency and duration.

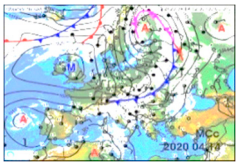
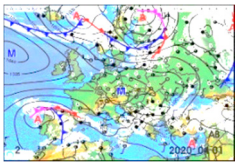
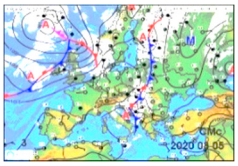
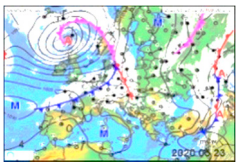
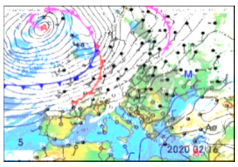
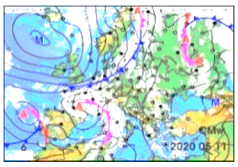
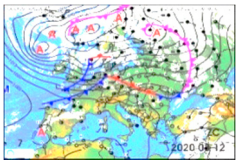
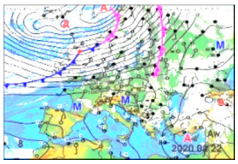
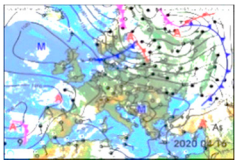
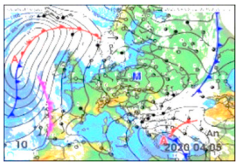
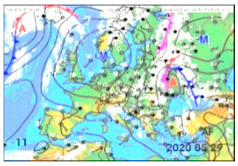
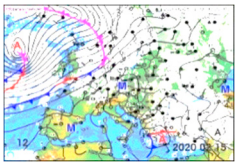
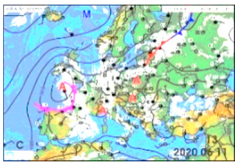
Types With Northern Current			
			
mCc (14.04.2020.)	AB (01.04.2020.)	CMc (05.08.2020.)	
Types with Southern Current			
			
mCw (23.06.2020.)	Ae (16.02.2020.)	CMw (11.05.2020.	
Types with Western Current			
			
zC (12.03.2020.)	Aw (22.02.2020.)	As (16.04.2020.)	
Types With Eastern Current		Types of Pressure Centers	
			
An (05.04.2020.)	AF (29.05.2020.)	A (15.02.2020.)	C (11.06.2020.)

Figure 1. The 13 macro-circulation types. All examples are taken from the year 2020. Within the maps, A means low pressure (cyclone) center, and M means high pressure (anticyclone) center.

The results in Section 3.2 will present the frequency distribution of selected weather extremes among the 13 circulation types. Grid-points A–I, selected to characterize extreme values in the Pannonian Basin, are presented in Figure 2. The coordinates of the central grid-point are 46.9 °N 20.4 °E with 1.5 deg. longitude or 1.0 deg. latitude difference between the neighboring grid-points. These differences correspond to ca. 100 × 100 km spatial resolution. Five grid-points fall into Hungary, two of them into Romania and one each into Serbia and Croatia.

The nine grid-point data are taken from the CarpatClim daily database [62,63]. CarpatClim is a freely available, high resolution gridded database. This database contains homogenized, interpolated, daily-scale meteorological parameters between 1961 and 2010. Climatological grids cover the area between latitudes 44 °N and 50 °N and longitudes 17 °E and 27 °E. Spatial resolution of the database is 0.1° × 0.1° geographical latitudes and longitudes, i.e., ca. 11 × 7 km in the region of our 9 grid-points. The CarpatClim database contains meteorological data for various parts of seven countries including Croatia, Hungary, Poland, Romania, Serbia, Slovakia and Ukraine.

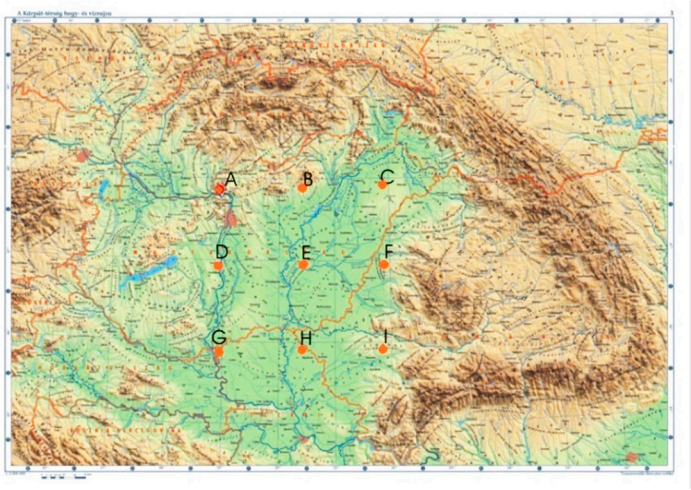


Figure 2. Location of the nine grid-points in the Pannonian Basin used for extreme values. The locations of the grid-points are indicated by the points below the capital letters, A–I.

The gridded database has been created from the observed data at the meteorological stations by homogenization (MASH) and interpolation procedure (MISH) [64].

Technical details (e.g., types of observing devices and number of stations) are detailed in [65], grouped according to the participating countries and the meteorological variables.

The central months of each season, i.e., January, April, July and October are presented, only. Note that in Section 3.3 the seasons mean the conventional three-monthly periods, i.e., December–February for winter, March–May for spring, June–August for summer and September–November for autumn.

By selection of the grid-points, we intended to characterize mostly the plain areas of the Pannonian Basin. Therefore, seven grid-points, from the selected nine, correspond to 73–136 m altitude above sea level. Only the points A and B have 549 and 233 m altitude, respectively. Since even point A does not really represent a mountainous area, we did not specifically analyze the differences among the nine grid-points.

Extremity is defined by the 5% threshold values comprehended in Table 2. Higher than the upper thresholds are investigated for daily precipitation, maximum temperature and wind speed values, whereas for the minimum temperature, the values cooler than the lower 5% thresholds are analyzed.

Table 2. Extremity (5% occurrence) thresholds of the investigated climate variables in the nine grid-points in 1961–2010.

Variable	Month	A	B	C	D	E	F	G	H	I
High Preci-pitation (mm/day)	Jan	5.1	8.6	5.2	5.1	3.9	4.2	4.7	3.9	6.9
	Apr	12.1	15.3	8.6	8.7	8.2	8.8	7.5	9.9	9.7
	July	19.3	21.3	16.6	15.4	18.2	15.3	13.8	16.2	14.2
	Oct	9.4	14.8	11.4	7.5	7.3	7.2	6.3	6.7	9.8
High Tmax (°C)	Jan	8.9	2.6	3.8	8.4	6.1	4.9	6.6	9.5	10.9
	Apr	20.1	10.3	16.3	22.0	18.4	18.0	21.9	23.9	23.6
	July	27.9	18.6	24.9	29.7	26.1	26.5	30.0	31.9	32.1
	Oct	20.4	15.1	17.6	21.5	17.7	18.7	20.8	23.2	22.9
Low Tmin (°C)	Jan	−18.8	−22.1	−20.7	−20.2	−22.7	−18.6	−20.1	−17.9	−13.2
	Apr	−2.4	−9.9	−6.3	−2.2	−6.1	−4.6	−2.4	−0.7	−0.5
	July	8.2	2.6	4.2	8.7	5.5	7.2	9.0	10.8	9.4
	Oct	−2.8	−8.6	−6.8	−3.2	−6.1	−4.4	−3.1	−1.9	−1.4
Strong Wind (m/s)	Jan	8.2	6.2	5.4	9.7	11.2	8.8	12.7	8.1	7.2
	Apr	5.2	8.2	6.3	7.6	7.1	8.6	8.6	7.5	7.9
	July	4.3	6.4	4.9	5.7	7.0	6.5	6.8	6.5	5.5
	Oct	6.0	7.0	5.2	7.4	7.8	7.2	8.6	6.7	5.9

The applied 5% threshold values are presented in Table 2 for the nine grid-points displayed in Figure 2. In addition to it, the absolute maxima or minima for the same nine grid-points are included in Table 3. The values of both Tables are derived independently from the circulation codes, and they can be considered important additions to the climate of the Pannonian Basin.

Table 3. Absolute extreme values of the investigated climate variables in nine grid-points in 1961–2010.

Variable	Month	A	B	C	D	E	F	G	H	I
High Preci-pitation (mm/day)	Jan	21.0	40.0	15.8	23.8	18.0	15.6	19.6	18.7	35.5
	Apr	53.7	56.8	21.4	40.7	45.7	37.6	31.8	40.3	41.0
	July	98.3	74.0	50.0	64.5	82.0	74.5	103.6	66.0	57.2
	Oct	37.8	52.8	39.0	39.7	27.7	27.8	34.6	28.9	40.5
High Tmax (°C)	Jan	13.8	7.8	8.5	14.7	11.4	9.5	12.3	15.9	16.9
	Apr	25.3	15.0	20.2	27.2	22.6	23.4	26.8	28.8	28.4
	July	33.1	23.2	28.9	34.8	30.8	31.4	34.2	37.2	38.6
	Oct	25.8	19.5	22.3	27.7	24.2	24.5	27.0	29.9	26.3
Low Tmin (°C)	Jan	−26.7	−32.4	−32.1	−32.2	−33.3	−29.8	−31.4	−28.9	−23.0
	Apr	−8.4	−15.2	−12.1	−10.2	−14.0	−9.0	−11.3	−10.2	−5.3
	July	4.9	−0.6	0.6	5.7	2.2	4.0	5.9	8.0	4.6
	Oct	−8.6	−15.6	−15.5	−9.9	−14.6	−11.4	−9.0	−7.4	−9.4
Strong Wind (m/s)	Jan	15.6	14.0	14.5	19.5	28.3	21.4	26.7	32.4	15.5
	Apr	12.0	17.3	11.2	14.9	16.2	14.5	17.4	14.8	15.1
	July	12.7	14.1	10.1	19.1	21.7	19.6	21.3	20.3	10.1
	Oct	17.0	17.2	12.5	19.2	22.4	19.0	21.5	16.7	15.2

The results presented in Section 3.2 indicate the distributions of the 5% extremes among the 13 circulation types calculated as the average of the nine grid-points in the central months of each season.

The last part of the investigations, detailed in Section 3.3, is the linear trend analysis of the original circulation types in the preliminarily selected 50 years (1971–2020) of monotonic increase of annual mean hemispherical averages of near-surface air temperature, together with three 30-year periods, characterized by neutral (1881–1910), warming (1911–1940), and cooling (1941–1970) periods, as presented in Figure 3. The most important Northern Hemispherical values, characterizing the above 30- and 50-year periods are included in Table 4. The regression coefficients of this Table are expressed in °C/10 years.

Table 4. Correlation and regression coefficients of the annual mean hemispherical temperature in one 50- and three 30-year periods.

Periods	Duration	Correlation	Regression (°C/10 Years)	NH Trend
1881–1910	30 years	0.002	0.0002	neutral
1911–1940	30 years	0.843	0.20	warming
1941–1970	30 years	−0.503	−0.07	cooling
1971–2020	50 years	0.954	0.28	warming

Investigated periods: 1881–1910, 1911–1940, 1941–1970, 1971–2020.

As concerns the longest monotonous period of 50 years, its warming tendency is "very likely" influenced by the increasing concentration of greenhouse gases [16]. Hence, this 50-year period can be treated as a natural experiment, simulating regional features of global warming. The external factors of the shorter warming, cooling, and neutral periods are most likely influenced by different global reasons.

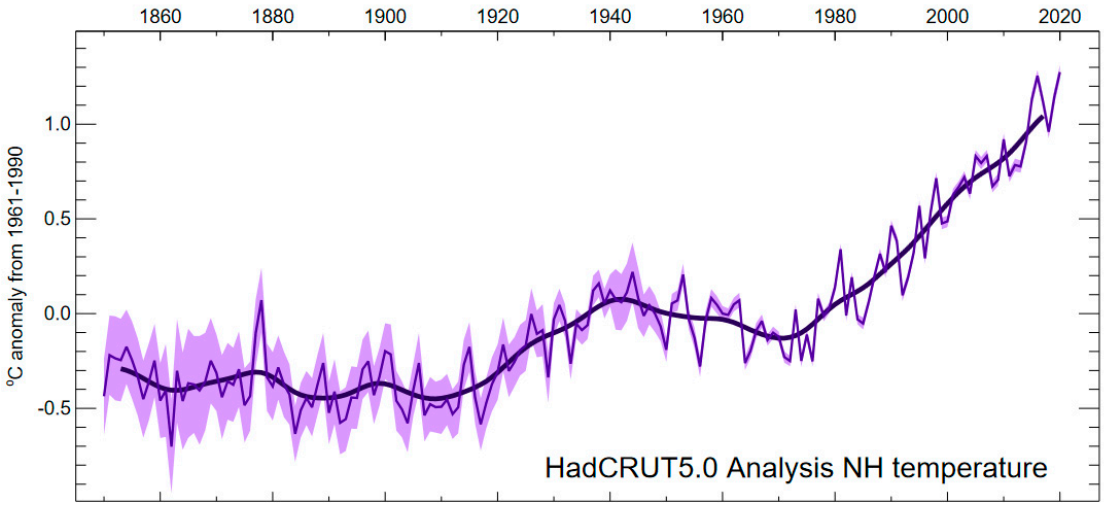


Figure 3. Anomalies of Northern Hemisphere annual surface air temperature since 1850 according to Hadley CRUT, a cooperative effort between the Hadley Center for Climate Prediction and Research and the University of East Anglia's Climatic Research Unit (CRU), UK. The source of information is https://crudata.uea.ac.uk/cru/data/temperature/HadCRUT5.0Analysis.pdf (accessed on 15 July 2021). The link for the licensing conditions is seen in the description of [66], in the list of References.

Finally, the significance of the linear trends for the local circulation frequency in the 50 years were established if both the correlation coefficients and the linear regression coefficient were significant according to the Z-test (Table A9 in [67]) and t-test [68] applied by SPSS, respectively. Since these two tests were statistically significant, for the same circulation types and seasons in the 50-year period, further below significance according to the correlation coefficients were considered in case of the 30-year periods, too. The 95% significance threshold for the correlation coefficients is 0.27 for the 50-year samples and 0.35 for the 30-year samples.

3. Results

3.1. Monthly Mean Frequency and Duration of the Circulation Types

The frequency distribution among the circulation types and the average duration are often applied characteristics of synoptic climatology. Table 5 and Figure 4 present these values for the 13 types in monthly resolutions. In the case of the frequency distribution, the annual mean values are also presented.

Table 5. Monthly and annual relative frequency (%) of the individual circulation types.

Type	Jan	Feb	Mar	Apr	May	June	July	Aug	Sep	Oct	Nov	Dec	Year
mCc	11	13	14	19	21	17	18	14	16	16	16	10	16
AB	8	6	11	8	8	11	7	6	7	6	5	6	8
CMc	1	1	1	2	1	1	1	1	1	1	2	1	1
mCw	9	9	9	6	5	4	2	2	5	5	6	8	5
Ae	12	12	13	11	7	7	7	9	13	18	23	14	12
CMw	9	9	7	10	6	4	2	2	5	7	12	12	7
zC	4	3	3	1	0	0	1	0	1	2	2	4	2
Aw	12	14	12	8	9	17	23	18	14	9	9	12	13
As	8	7	4	4	5	4	3	2	3	5	5	7	4
An	10	7	9	11	14	9	10	16	13	9	5	7	10
AF	1	5	4	7	8	5	6	8	7	7	2	3	6
A	14	11	10	7	9	14	14	16	12	12	11	15	12
C	2	3	4	6	6	7	6	4	4	3	2	2	4
All	100	100	100	100	100	100	100	100	100	100	100	100	100

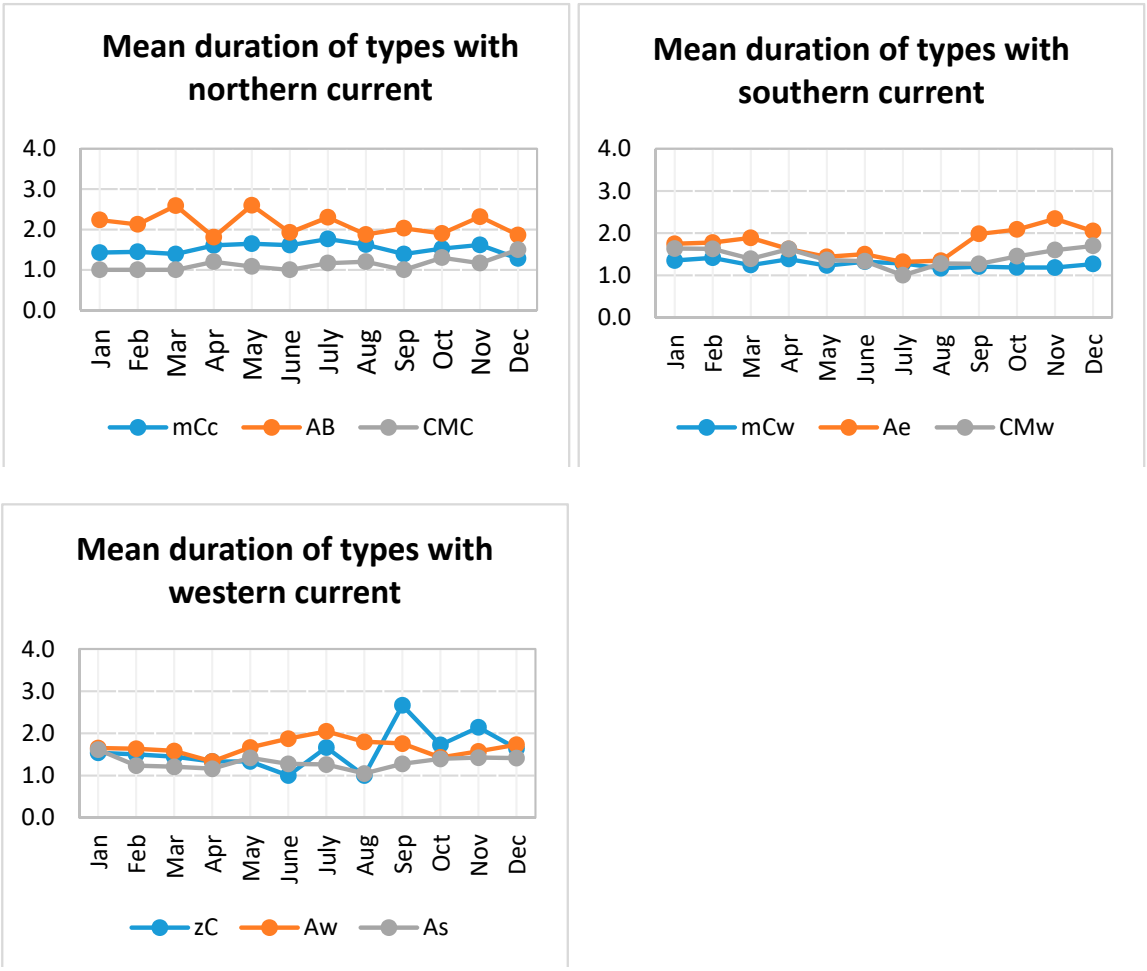


Figure 4. Monthly mean duration of the macro-synoptic types as grouped by Peczely (1957) according to the wind direction in the Pannonian Basin.

The average duration of the circulation types (Figure 4) is grouped according to Peczely [1,2], considering the main direction of near-surface wind, as displayed above in Table 1.

The smallest average duration can be 1.0 days, which occurs when all appearances of the given type remain valid for one day only. This situation is valid in several months for the CMc type with 1–2 months of occurrence for CMw, zC, and C types. The anticyclones mostly represent the longest duration of the given wind direction group with a characteristic duration of 1.5–2.5 days on average. The only exception to this is the type zC in September, which had over 2.5 days' average duration.

3.2. Distribution of Weather Extremes among the Circulation Types

Distribution of selected daily extreme values have been analyzed in nine grid-points presented above in Figure 2. High precipitation, high diurnal temperature maxima, low diurnal minima, and high diurnal wind speed values are considered. Threshold values of the 5% frequency and the absolute maxima are presented above in Tables 2 and 3, respectively.

In this sub-Section, the frequency distributions that occurred in all nine grid-points are presented in Figure 5. The four units of the Figure represent the selected extreme events in the central months of every season. Within all units, the columns represent the frequency of occurrence averaged for the nine grid-points.

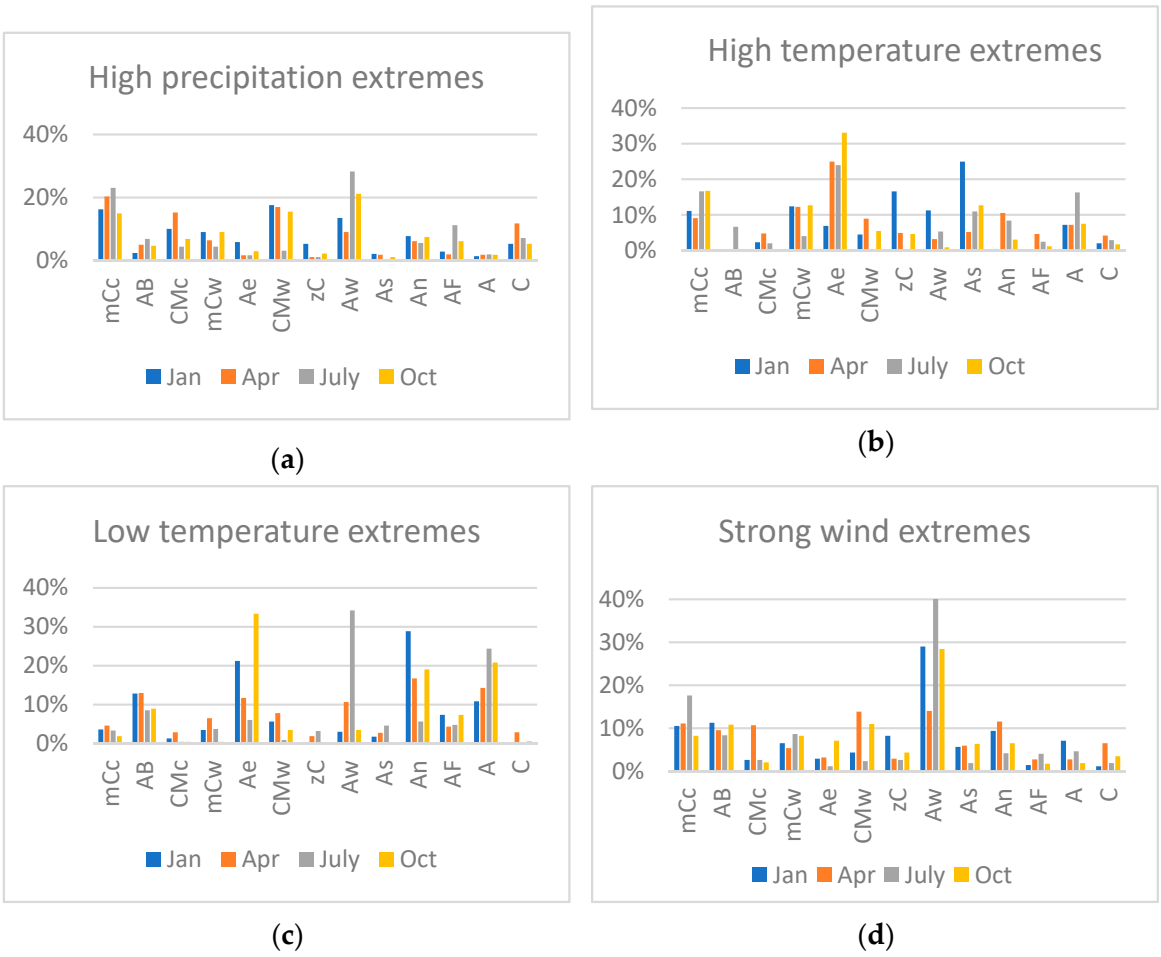


Figure 5. Distribution of the 5% extreme days among the macro-circulation types on average of the nine investigated grid-points: (**a**) high precipitation, (**b**) high maximum temperature, (**c**) low minimum temperature, and (**d**) high wind speed.

The high diurnal precipitation sums occur most frequently in mCc, CMw, and Aw, whereas rather rarely in the zC, As, and A macro-circulation types. The high frequency of much rain in the Aw situation is not surprising, as in the praxis of storm warning for the Lake Balaton this is a dangerous situation if a hidden cold front is contained by the so-called "nose of the anticyclone" spreading ahead from the main body of the high pressure to the west from the Pannonian Basin [69]. Otherwise, one can establish that almost all macro-circulation types may be accompanied by heavy rains in all central months of the seasons.

For the daily wind speed (averaged for the whole day from 10 min periods) similar behavior can be established: the diurnal wind speed maxima occur in almost each original circulation type in each investigated month. The highest proportion of extremely strong winds occur in the Aw types of circulation. In July this frequency reached 40%, which means that this proportion of the extremes occur in days with this type of circulation.

As concerns the temperature extremes, there are several macro-circulation types and seasons when no extreme values occur in any of the nine grid-points. For both the high maximum temperatures and for the low minimum temperatures, there are six types for both temperature extremes when no extreme occurs in one, two, or three investigated months. The highest maximum temperature extremes occur in the days with Ae types, whereas for the lowest temperature minima are different in the different investigated months. In July and in October over 30% of these extremes belong to Aw and Ae types, respectively.

3.3. Trends in Monotonous Hemispherical Warming and Cooling Periods

From the period 1971–2020, only those circulation types are involved in the following Figures and Tables that are significant according to both the correlation and the regression coefficients. As can be seen in Table 6, these two criteria coincide for both statistical parameters. In other words, both parameters found identical seasons and circulation types to be significant. More exactly, the Table indicates identical numbers of significance of both coefficients in each season. The pair-wise equivalence of significance could be established from the detailed matrices of significance according to the two statistical indicators.

Table 6. Significance (95%) of seasonal linear trends of circulation in the 1971–2020 global warming period according to the correlation and the regression coefficients. Note that the seasons are three-monthly periods, i.e., December–February for winter, March–May for spring, etc.

Original Circulation Types (Frequency from 13 Types)					
Significance according to	Winter	Spring	Summer	Autumn	Percentage
Correlation	4	6	5	4	37%
Regression	4	6	5	4	37%

As can be seen from Table 6, 37% of the original types are significant. This means 19 significant trends from the 13 types × four seasons = 52 possible investigated coefficients. The 19 coefficients are the sum of the corresponding lines in the table, indicated in the various seasons.

The 37% of the significant linear trends is much higher than the random occurrence (5%). Hence, in Figures 6–9, the graphs of significant linear trends are presented with the best fitted linear regression lines. The four figures contain the seasonal trends of frequency from winter to autumn. The numerical values of these linear trends are presented later in this Section.

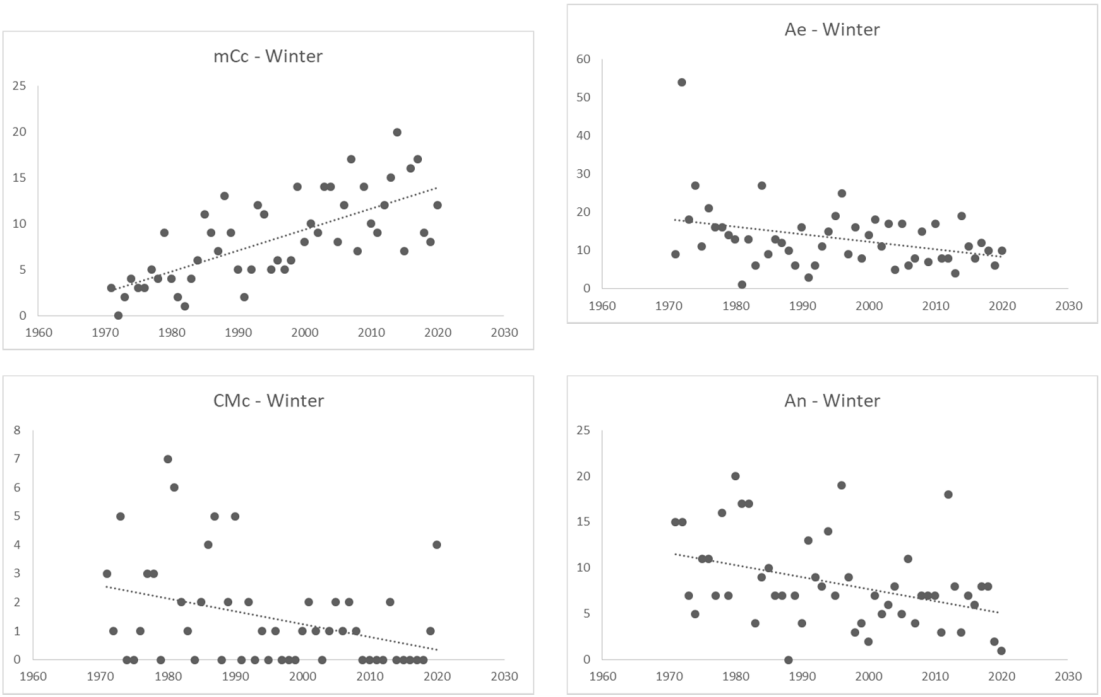


Figure 6. Significant linear trends in frequency of the various macro-circulation types in the 1971–2020 monotonically warming period. Winter.

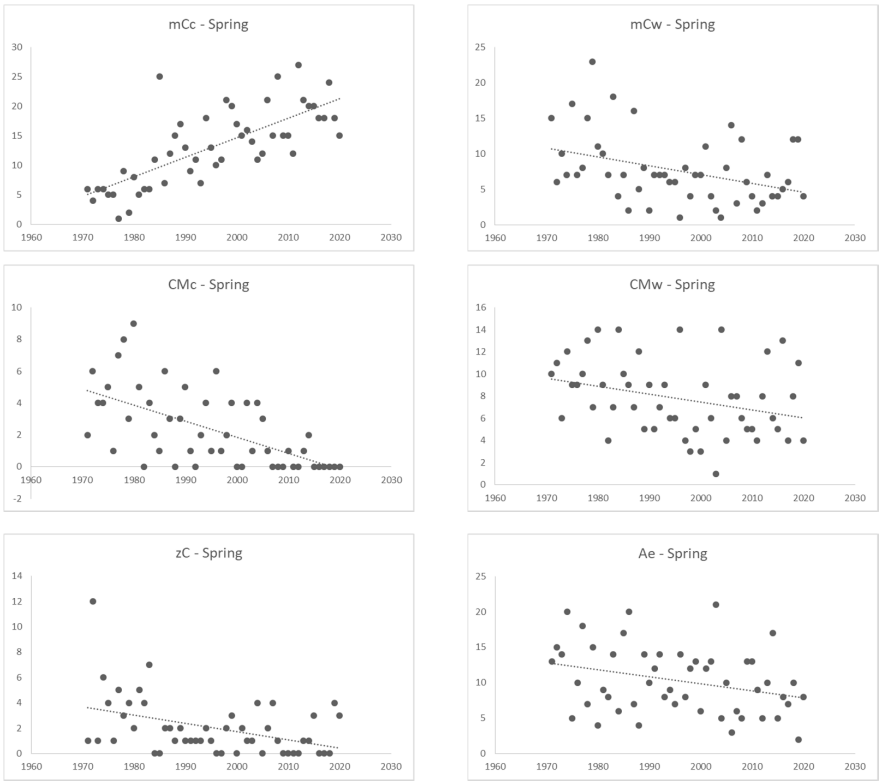


Figure 7. Significant linear trends in frequency of the various macro-circulation types in the 1971–2020 monotonically warming period. Spring.

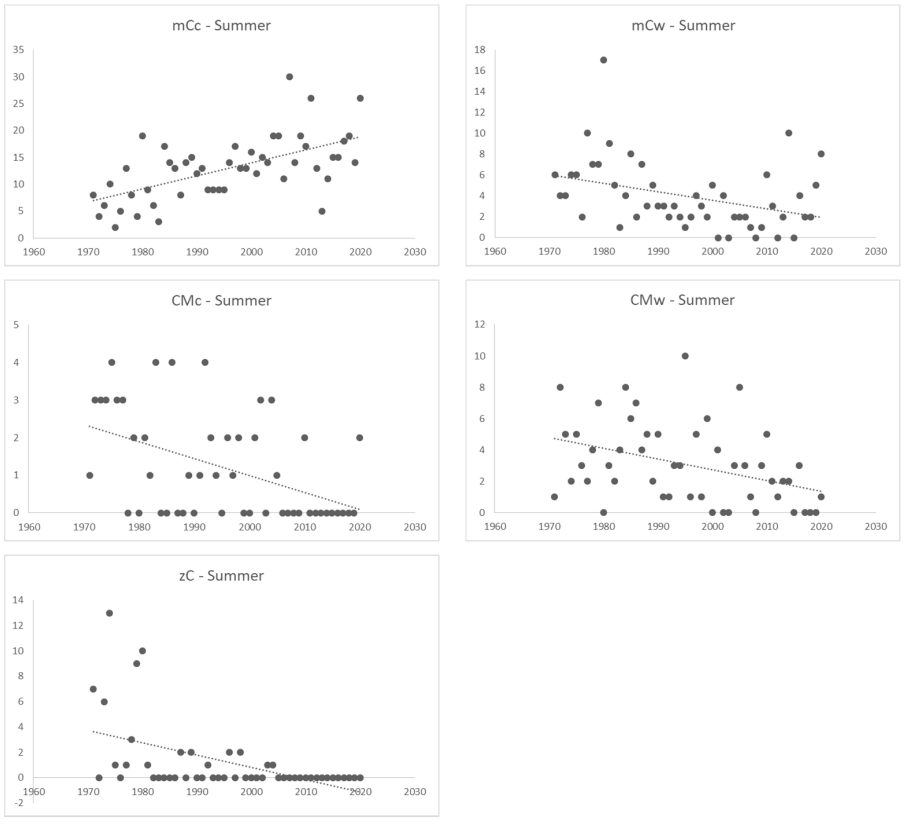


Figure 8. Significant linear trends in frequency of the various macro-circulation types in the 1971–2020 monotonically warming period. Summer.

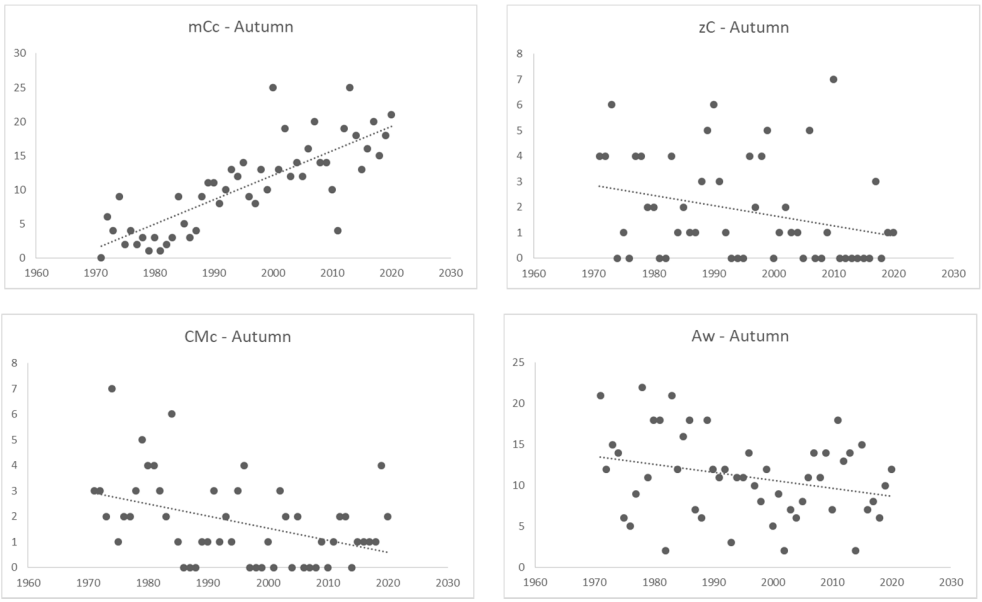


Figure 9. Significant linear trends in frequency of the various macro-circulation types in the 1971–2020 monotonically warming period. Autumn.

Figures 6–9 display the seasonal linear trends found equally significant according to both tests concerning correlation (Z-test) and regression (*t*-test) described in Section 2. Only eight macro-synoptic types exhibit significant frequency trends in any of the seasons (see below), and in five types there are no significant trends at all. They are the AB, As, AF, A, and C types.

There are only two types that have significant linear trends in all four seasons. These types are the mCc (increasing) and CMc (decreasing), which exhibit significant trends in all seasons. The zC is represented by a significant trend in three seasons. Three types, mCw, Ae, and CMw, exhibit significant trends in two seasons, whereas An is characterized by a significant trend only in one season. As mentioned above, all the trends from zC to An are negative (decreasing).

It is worth mentioning that for a given type, the signs of the significant trends are the same in all seasons. From the total of 19 significant coefficients in the four seasons, only mCc exhibits an increasing linear trend, whereas the other seven types are characterized by decreasing trends parallel to the hemispherical warming in 1971–2020.

Concerning the above statistically established increasing and decreasing trends in the recent 50 years, it would be ideal if one could establish whether or not they are direct consequences of hemispherical warming. This question can finally be answered by climate modelling, which is not available for the authors of the present paper. Therefore, in the last two Tables of this study the circulation frequency trends are also established for the other three 30-year periods specified in Table 4 of Section 2. The three periods, taken from the latter Table, are the neutral 1881–2010, the warming 1911–1940, and the cooling 1941–1970 years, based on hemispherical mean temperature, in the hope that the warming 30 years produce trends similar to the 50 years of warming, and the cooling 30 years yields opposite results, with no significant circulation trends in the neutral 30 years.

Table 7 presents the proportions of significant linear trends of circulation types in these 30-year periods for comparison to the trends in the recent 1971–2020 period. One can establish that the proportions of significant linear trends are much smaller: 10 and 13% for the shorter warming and cooling periods, respectively. In addition to this, the neutral period exhibits similarly low frequency, 12%.

Table 7. The number of significant seasonal correlation coefficients of the linear trends in the four time periods, defined according to the Northern Hemisphere temperature presented in Table 4.

Significance in	NH Correl.	Winter	Spring	Summer	Autumn	Percent
1881–1910	0.002	1	2	0	3	12%
1911–1940	0.843	2	1	1	1	10%
1941–1970	−0.503	0	4	2	1	13%
1971–2020	0.954	4	6	5	4	37%

The significant regression coefficients are presented for the 13 types in Table 8. For the 30-year periods, only those circulation types and seasons are included that are significant in the 50-year period.

Table 8. Significant trends of those circulation types and seasons that were significant in the 1971–2020 period. The significant values that are of appropriate sign (i.e., identical in the warming 1911–1940 and opposing in the cooling 1941–1970 period) are set in *italics.*

	Circulation Types Found Significant in 1971–2020	Frequency Trend (yr^{-1}) 1881–1910 $R(T_{NH}) = 0.002$	Frequency Trend (yr^{-1}) 1911–1940 $R(T_{NH}) = 0.843$	Frequency Trend (yr^{-1}) 1941–1970 $R(T_{NH}) = -0.503$	Frequency Trend (yr^{-1}) 1971–2020 $R(T_{NH}) = 0.954$
Winter	mCc				+0.228
	CMc		+0.086		−0.045
	Ae				−0.196
	An				−0.132
Spring	mCc				+0.331
	CMc			*+0.100*	−0.101
	mCw				−0.123
	Ae		*−0.335*		−0.098
	CMw	+0.233		*+0.073*	−0.071
	zC				−0.065
Summer	mCc				+0.242
	CMc			*+0.109*	−0.045
	mCw				−0.081
	CMw				−0.069
	zC				−0.907
Autumn	mCc				+0.358
	CMc				−0.047
	zC				−0.040
	Aw	−0.236			−0.096

From the latter 19 regression coefficients, found significant for the 13 circulation types in 1971–2020, there are only seven that are significant in any other 30-year period. From these coefficients, five occurred in warming or cooling periods, signs of which are appropriate in four cases, only (Table 8).

In summary, we can conclude that the relatively high 37% proportion of significant tendencies in the circulation frequency are much higher than their random occurrence. However, the question of whether or not these trends are universal consequences of the hemispherical warming is discussed below.

4. Discussion

As was mentioned in the Introduction, both empirical and objective methods are applied to establish circulation classifications and their daily coding. In the case of empirical coding of the Peczely types, it is advantageous that the coding is performed by two experts, only, who even worked together as a professor and his assistant for some years [3].

Monthly mean relative frequencies and durations are presented for the most recent 30-year period (1991–2020). Although these values are often published [8,9,13,15] based on various time sequences, the values presented in this paper are the most recent ones for a standard 30-year period.

The interesting difference between the distribution of precipitation and wind extremes, on one side, and the temperature maxima and minima, on the other side are that the extremes of the first group may occur practically in all circulation types, whereas those on the second side occur in all seasons only in seven types. In other words, there are six types from the 13, where in one, two or three season-central months where no 5% extremes occur.

The most likely explanation of this behavior is that the lifetime of the mesoscale objects leading to heavy rain and strong wind is much shorter than the 24 h for which the macro-synoptic codes are defined [5,69,70]. This means that these mesoscale objects may develop practically under any macro-synoptic code. On the other hand, formation of the temperature extremes needs a longer time at the temperate latitudes, hence in case of several macro-synoptic situations the conditions are not favorable for the temperature extremes.

The applied 50-year (1971–2020) period exhibits a steep hemispherical warming tendency (+0.28 °C/10 yr) also characterized by a very high (0.954) correlation coefficient. The previous warming period (1911–1940) also exhibits steep (+0.20 °C/10 yr) regressions and high (0.843) correlation coefficients. Both periods are recommended to use as first approximations of regional features for global climate change, although the set of external forcing factors are probably different in the two warming periods [16].

Concerning the frequency trends analyzed in the recent 50 years (1971–2020) there are three questions to discuss: (i) How are the significant trends related to the former analyses of circulation changes? (ii) Can we validate these trends by performing a similar investigation for shorter time periods? (iii) How could one involve the climate models in such a validation process?

In relation to (i), one can establish that 37% of the 13 macro-types and seasons provided significant trends at the 95% significance level, which is much more than their random occurrence, i.e., 5%. However, the former expectations for the increase in persistent circulation [58–61] parallel to global warming are not supported by our results, which rather support the conclusions of [56,57], stating seasonal differences in the statistical investigations and a lack of unequivocal changes in the circulation projected by global climate models.

Concerning (ii), we should establish that the circulation frequency trends of the shorter periods occur much more rarely than in the 50-year period. This means that by using only this statistical technique of linear trend analysis, we cannot decide whether or not they are universal consequences of global warming. Even if the proportion of significant trends is much smaller, the external forcing factors can also be sources of these big differences between the results of the 50-year period and the 30-year periods.

For question (iii), objective classification of the daily weather maps [52–55] would be very useful, especially in terms of those meteorological fields that are available in the climate models. Here, both the General Circulation Models (GCM) and the Regional Climate Models (RCM) can be considered. Validation of climate models in terms of circulation and the physical reasoning of the derived frequency trends could be performed based on this objective classification.

The significant trends in frequency of the macro-synoptic types (Figures 6–9) can be combined with the occurrence of weather extremes in the various macro-types (Figure 5) to assess how the frequency of the given weather extremes are expected to change parallel to global warming. For example, the observed increase in type mCc in all seasons during the recent 50 years may increase the frequency of high precipitation events in the future. However, as mentioned above in this Section, one cannot be sure that the observed circulation trends are universal consequences of global warming.

5. Conclusions

Finally, let us briefly list the conclusions of the presented investigations:

As the result of subjective coding by only two experts, one of the longest diurnal series of macro-circulation series exist for the Pannonian Basin.

The monthly frequency and duration statistics are available for each of the 13 macro-synoptic types for the last 30 years' standard period (1991–2020).

Nine grid-points are selected from the CarpatClim database to obtain a ca. 100 × 100 km resolution network to identify four diurnal weather extremes in the central months of each season and to establish their occurrence parallel to the macro-circulation types. The 5% threshold values and the absolute extremity are presented for each grid-point.

The distribution of 5% extreme values among the macro-circulation types is presented as the average of the nine grid-points. An unexpected difference was found between distribution of precipitation and wind extremes, on one hand, and the temperature maxima and minima, on the other hand. More specifically, the extremes of the first group may occur practically in all circulation types, whereas those of the second group are concentrated in seven circulation types with no appearance in one–three season-center months in the other six types. For the likely reason for this difference, see the Discussion.

One 50-year period (1971–2020), characterized by monotonous hemispherical warming, has been defined, as well as three 30-year sequences of warming (1911–1940), cooling (1941–1970), and neutral (1881–1910) periods. They are tackled as natural experiments for expected further global warming. This approach, however, has not been supported by our trend estimations, as is discussed in Section 4. Therefore, the established trends detected in the circulation types can be considered facts of the given 50-year period but not necessarily general consequences of global warming, as discussed in Section 4.

Author Contributions: J.M. carried out the conceptualization and the majority of the statistical computations. C.K. provided the daily codes of the macro-types, selected and created Figures 1 and 2, and collected most of the Hungarian references. L.L. contributed with research ideas, provided or improved parts of figures, and significantly contributed to the collection and evaluation of the international references. All authors have read and agreed to the published version of the manuscript.

Funding: This research received no external funding.

Institutional Review Board Statement: Not applicable.

Informed Consent Statement: Not applicable.

Data Availability Statement: Reference [3] contains all daily codes until 2015. Further codes and the older codes in convenient data format are freely available from the author upon request. Availability is ensured for the other types of local and hemispherical data in the provided references.

Conflicts of Interest: The authors declare no conflict of interest.

References

1. Peczely, G. Grosswetterlagen in Ungarn. *Kleinere Veröffentlichungen Zent. Für Meteorol.* **1957**, *30*.
2. Péczely, G. Catalogue of macro-synoptic types for Hungary (1881-1983). *Országos Meteorológiai Szolgálat Kisebb Kiadványai* **1983**, *53*.
3. Károssy, C. Catalogue of Peczely macro-synoptic types for the Carpathian Basin, 1881-2015. *Légkör* **2018**, *63*, 11–40. (In Hungarian)
4. van Bebber, W.J.; Köppen, W. Die Isobartypen des Nordatlantischen Ozeans und Westeuropas, ihre Bezeihung zur Lage und Bewegung der Barometrischen Maxima und Minima. *Arch. Dtsch. Seewarte* **1895**, *18*, 27.
5. Barry, R.G.; Perry, A.H. *Synoptic Climatology*; Methuen & Co. Ltd.: London, UK, 1973; p. 555.
6. Bower, D.; Glenn, R.; McGregor-Hannah, D.; Sheridan, C. Development of a spatial synoptic classification scheme for Western Europe. *Int. J. Climatol.* **2007**, *27*, 2017–2040. [CrossRef]
7. Maheras, P.; Tolika, K.; Tegoulias, I.; Anagnostopoulou, C.; Szpirosz, K.; Károssy, C. Comparison of automatic and emprirical classification of circulation types based on data from Hungary. *Légkör* **2017**, *62*, 60–67. (In Hungarian)
8. Makra, L.; Mika, J.; Juhász, M.; Mika, J.; Bartzokas, A.; Bérczi, R.; Sümeghy, Z. Relationship between the Péczely's largescale weather types and airborne pollen grain concentrations for Szeged, Hungary. *Grana* **2007**, *46*, 43–56. [CrossRef]
9. Kiss, Á.; Károssy, C. Charakteristiken der Tagesschwankung der Temperatur auf dem südlichen Teil der ungarischen Tiefebene. *Acta Climatol. Acta Univ. Szeged.* **1973**, *12*, 19–46.
10. Maller, A.; Németh, E.; Rimek, I.; Török, L.; Varga, L. Areal precipitation distributions in several circulation patterns and medium range probabilistic precipitation forecasts. *Idôjárás* **1990**, *94*, 108–123. (In Hungarian)
11. Lakatos, M.; Ferenczi, Z. Investigation of background air pollution in connection with circulation conditions over Hungary. In Proceedings of the "Geophysics and Environment: Background Air Pollution" Meeting, Rome, Italy, 16–18 June 1992.
12. Károssy, C. Peczely's catalogue of macrosynoptic types (1983–1987). *Légkör* **1987**, *32*, 28–30. (In Hungarian)

13. Károssy, C. Péczely's classification of macrosynoptic types and catalogue of weather situations (1996-2000). In *Light Trapping of Insects Influenced by Abiotic Factors*; Part III; Nowinszky, L., Ed.; OSKAR: Szombathely, Hungary, 2001; pp. 117–130.
14. Matyasovszky, I.; Weidinger, T. Charaterizing air pollution potential over Budapest using macrocirculation types. *Időjárás* **1998**, *102*, 219–237.
15. Mika, J.; Szentimrey, T.; Domonkos, P.; Rimóczi-Paál, A.; Károssy, C. Approximating climatic representativity for satellite samples of limited length. *Adv. Space Res.* **1993**, *14*, 125–128. [CrossRef]
16. USGCRP. *Climate Science Special Report: Fourth National Climate Assessment*; Wuebbles, D.J., Fahey, D.W., Hibbard, K.A., Dokken, D.J., Stewart, B.C., Maycock, T.K., Eds.; U.S. Global Change Research Program: Washington, DC, USA, 2017; Volume 1, p. 470. Available online: https://science2017.globalchange.gov/ (accessed on 11 November 2017).
17. Fischer, E.; Knutti, R. Anthropogenic contributions to global occurrence of heavy-precipitation and high-temperature extremes. *Nat. Clim. Chang.* **2015**, *5*, 560–564. [CrossRef]
18. Schleussner, C.-F.; Lissner, T.K.; Fischer, E.M.; Wohland, J.; Perrette, M.; Golly, A.; Rogelj, J.; Childers, K.; Schewe, J.; Frieler, K.; et al. ifferential climate impacts for policy-relevant limits to global warming: The case of 1.5 °C and 2 °C. *Earth Syst. Dynam. Discuss* **2015**, *6*, 2447–2505. Available online: www.earth-syst-dynam-discuss.net/6/2447/2015/ (accessed on 27 October 2020).
19. Schleussner, C.-F.; Lissner, T.K.; Fischer, E.M.; Wohland, J.; Perrette, M.; Golly, A.; Rogelj, J.; Childers, K.; Schewe, J.; Frieler, K.; et al. Supplement of Differential climate impacts for policy-relevant limits to global warming: The case of 1.5 °C and 2 °C. *Earth Syst. Dynam.* **2016**, *7*, 327–351. [CrossRef]
20. James, R.; Washington, R.; Schleussner, C.-F.; Rogelj, J.; Conway, D. Characterizing half-a-degree difference: A review of methods for identifying regional climate responses to global warming targets. *Wiley Interdiscip. Rev. Clim. Chang.* **2017**, *8*, e457. [CrossRef]
21. Schewe, J.; Levermann, A. Non-linear intensification of Sahel rainfall as a possible dynamic response to future warming. *Earth Syst. Dyn.* **2017**, *8*, 495–505. [CrossRef]
22. Whan, K.; Zscheischler, J.; Orth, R.; Shongwe, M.; Rahimi, M.; Asare, E.O.; Seneviratne, S.I. Impact of soil moisture on extreme maximum temperatures in Europe. *Weather Clim. Extrem.* **2015**, *9*, 57–67. [CrossRef]
23. Francis, J.A.; Vavrus, S.J.; Cohen, J. Amplified Arctic warming and mid-latitude weather: Emerging connections. *Wiley Interdiscip. Rev. Clim. Chang.* **2017**, *8*, e474. [CrossRef]
24. Kennedy, D.; Parker, T.; Woollings, T.; Harvey, B.; Shaffrey, L. The response of high-impact blocking weather systems to climate change. *Geophys. Res. Lett.* **2016**, *43*, 7250–7258. [CrossRef]
25. Norris, J.R.; Allen, J.R.; Evan, A.T.; Zelinka, M.D.; O'Dell, C.W.; Klein, S.A. Evidence for climate change in the satellite cloud record. *Nature* **2016**, *536*, 72–75. [CrossRef] [PubMed]
26. Nilsen, I.B.; Stagge, J.H.; Tallaksen, L.M. A probabilistic approach for attributing temperature changes to synoptic type frequency. *Int. J. Climatol.* **2017**, *37*, 2990–3002. [CrossRef]
27. Wirth, S.B.; Glur, L.; Gilli, A.; Anselmetti, F.S. Holocene flood frequency across the Central Alps—Solar forcing and evidence for variations in North Atlantic atmospheric circulation. *Quat. Sci. Rev.* **2013**, *80*, 112–128. [CrossRef]
28. Orme, L.C.; Charman, D.J.; Reinhardt, L.; Jones, R.T.; Mitchell, F.J.G.; Stefanini, B.S.; Barkwith, A.; Ellis, M.A.; Grosvenor, M. Past changes in the North Atlantic storm track driven by insolation and sea-ice forcing. *Geology* **2017**, *45*, 335–338. [CrossRef]
29. Roberts, N.; Moreno, A.; Valero-Garces, B.L.; Corella, J.P.; Jones, M.; Allcock, S.; Woodbridge, J.; Morellon, M.; Luterbacher, J.; Xoplaki, E.; et al. Palaeolimnological evidence for an east–west climate see-saw in the Mediterranean since AD 900. *Glob. Planet. Chang.* **2012**, *84*, 23–34. [CrossRef]
30. Francis, J.A.; Vavrus, S.J. Evidence linking Arctic amplification to extreme weather in mid-latitudes. *Geophys. Res. Lett.* **2012**, *39*, L06801. [CrossRef]
31. Coumou, D.; Petoukhov, V.; Rahmstorf, S.; Petri, S.; Schellnhuber, H.J. Quasi-resonant circulation regimes and hemispheric synchronization of extreme weather in boreal summer. *Proc. Natl. Acad. Sci. USA* **2014**, *111*, 12331–12336. [CrossRef]
32. Haimberger, L.; Mayer, M. Global climate; Atmospheric circulation; Upper air wind. [in "State of the Climate in 2016"]. *Bull. Am. Meteorol. Soc.* **2017**, *98*, S39–S41.
33. Kornhuber, K.; Osprey, S.; Coumou, D.; Petri, S.; Petoukhov, V.; Rahmstorf, S.; Gray, L. Extreme weather events in early summer 2018 connected by a recurrent hemispheric wave-7 pattern. *Environ. Res. Lett.* **2019**, *14*, 054002. [CrossRef]
34. Chang, E.K.M.; Yau, A.M.W. Northern Hemisphere winter storm track trends since 1959 derived from multiple reanalysis datasets. *Clim. Dyn.* **2016**, *47*, 1435–1454. [CrossRef]
35. Wang, J.; Dai, A.; Mears, C. Global water vapor trend from 1988 to 2011 and its diurnal asymmetry based on GPS, radiosonde, and microwave satellite measurements. *J. Clim.* **2016**, *29*, 5205–5222. [CrossRef]
36. Neu, U.; Akperov, M.G.; Bellenbaum, N.; Benestad, R.; Blender, R.; Caballero, R.; Cocozza, A.; Dacre, H.F.; Feng, Y.; Fraedrich, K.; et al. IMILAST: A Community Effort to Intercompare Extratropical Cyclone Detection and Tracking Algorithms. *Bull. Am. Meteorol. Soc.* **2013**, *94*, 529–547. [CrossRef]
37. Wang, J.; Kim, H.M.; Chang, E.K.M. Changes in Northern Hemisphere winter storm tracks under the background of arctic amplification. *J. Clim.* **2017**, *30*, 3705–3724. [CrossRef]
38. Davini, P.; Cagnazzo, C.; Gualdi, S.; Navarra, A. Bidimensional diagnostics, variability, and trends of Northern Hemisphere blocking. *J. Clim.* **2012**, *25*, 6496–6509. [CrossRef]
39. Hanna, E.; Fettweis, X.; Hall, R.J. Recent changes in summer Greenland blocking captured by none of the CMIP5 models. *Cryosphere* **2018**, *12*, 3287–3292. [CrossRef]

40. Overland, J.; Francis, J.A.; Hall, R.; Hanna, E.; Kim, S.-J.; Vihma, T. The melting Arctic and midlatitude weather patterns: Are they connected? *J. Clim.* **2015**, *28*, 7917–7932. [CrossRef]
41. Yuan, J.; Li, W.; Deng, Y. Amplified subtropical stationary waves in boreal summer and their implications for regional water extremes. *Environ. Res. Lett.* **2015**, *10*, 104009. [CrossRef]
42. Wills, R.C.J.; White, R.H.; Levine, X.J. Northern Hemisphere Stationary Waves in a Changing Climate. *Curr. Clim. Chang. Rep.* **2019**, *5*, 372–389. [CrossRef] [PubMed]
43. Coumou, D.; Di Capua, G.; Vavrus, S.; Wang, L.; Wang, S. The influence of Arctic amplification on midlatitude summer circulation. *Nat. Commun.* **2018**, *9*, 2959. [CrossRef] [PubMed]
44. Sousa, P.M.; Trigo, R.M.; Barriopedro, D.; Soares, P.M.; Ramos, A.M.; Liberato, M.L. Responses of European precipitation distributions and regimes to different blocking locations. *Clim. Dyn.* **2017**, *48*, 1141–1160. [CrossRef]
45. Lenggenhager, S.; Croci-Maspoli, M.; Brönnimann, S.; Martius, O. On the dynamical coupling between atmospheric blocks and heavy precipitation events: A discussion of the southern Alpine flood in October 2000. *Q. J. R. Meteorol. Soc.* **2018**, *145*, 530–545. [CrossRef]
46. Schubert, S.D.; Wang, H.; Koster, R.D.; Suarez, M.J.; Groisman, P.Y. Northern Eurasian heat waves and droughts. *J. Clim.* **2014**, *27*, 3169–3207. [CrossRef]
47. Dunn-Sigouin, E.; Son, S.W. Northern Hemisphere blocking frequency and duration in the CMIP5 models. *J. Geophys. Res. Atmos.* **2013**, *118*, 1179–1188. [CrossRef]
48. Tilinina, N.; Gulev, S.K.; Bromwich, D. New view of Arctic cyclone activity from the Arctic System reanalysis. *Geophys. Res. Lett.* **2014**, *41*, 1766–1772. [CrossRef]
49. Tilinina, N.; Gulev, S.K.; Rudeva, I.; Koltermann, P. Comparing cyclone life cycle characteristics and their inter-annual variability in different reanalyzes. *J. Clim.* **2013**, *26*, 6419–6438. [CrossRef]
50. Hess, P.; Brezowsky, H. Catalogue of European Grosswetterlagen. *Ber. Des Dtsch. Wetterd.* **1977**, *15*, 68. (In German)
51. Werner, P.C.; Gerstengarbe, F.W. Catalogue of European Grosswetterlagen. Potsdam-Institut für Klimafolgenforschung. *PIK-Report* **2010**, *119*, 140. (In German)
52. Demuzere, M.; Werner, M.; van Lipzig, N.P.M.; Roeckner, E. An analysis of present and future ECHAM5 pressure fields using a classification of circulation patterns. *Int. J. Climatol.* **2009**, *29*, 1796–1810. [CrossRef]
53. Huth, R.; Beck, C.; Andreas, P.; Demuzere, M.; Ustrnul, Z.; Cahynova, M.; Kyselý, J.; Tveito, O.E. Classifications of atmospheric circulation patterns: Recent advances and applications. *Ann. N. Y. Acad Sci.* **2008**, *1146*, 105–152. [CrossRef]
54. Jones, P.D.; Harpham, C.; Briffa, K.R. Lamb weather types derived from reanalysis products. *Int. J. Climatol.* **2013**, *33*, 1129–1139. [CrossRef]
55. Kyselý, J.; Huth, R. Changes in atmospheric circulation over Europe detected by objective and subjective methods. *Theor. Appl. Climatol.* **2006**, *85*, 19–36. [CrossRef]
56. Bartoszek, K. The main characteristics of atmospheric circulation over East-Central Europe from 1871 to 2010. *Meteorol. Atmos. Phys.* **2017**, *129*, 113–129. [CrossRef]
57. Huguenin, M.F.; Fischer, E.M.; Kotlarski, S.; Scherrer, S.C.; Schwierz, C.; Knutti, R. Lack of change in the projected frequency and persistence of atmospheric circulation types over Central Europe. *Geophys. Res. Lett.* **2020**, *47*, e2019GL086132. [CrossRef]
58. Steirou, E.; Gerlitz, L.; Apel, H.; Merz, B. Links between large-scale circulation patterns and streamflow in Central Europe: A review. *J. Hydrol.* **2017**, *549*, 484–500. [CrossRef]
59. Jézéquel, A.; Cattiaux, J.; Naveau, P.; Radanovics, S.; Ribes, A.; Vautard, R.; Vrac, M.; Yiou, P. Trends of atmospheric circulation during singular hot days in Europe. *Environ. Res. Lett.* **2018**, *13*, 054007. [CrossRef]
60. Blackport, R.; Screen, J.A.; van der Wiel, K.; Bintanja, R. Coincident cold winters in mid-latitudes. *Nat. Clim. Chang.* **2019**, *9*, 697–704. [CrossRef]
61. Mori, M.; Kosaka, Y.; Watanabe, M.; Nakamura, H.; Kimoto, M. A reconciled estimate of the influence of Arctic Sea-ice loss on recent Eurasian cooling. *Nat. Clim. Chang.* **2019**, *9*, 123–129. [CrossRef]
62. The Carpatclim Data Base. Available online: http://www.carpatclim-eu.org/pages/download/ (accessed on 31 March 2021).
63. Spinoni, J.; Szalai, S.; Szentimrey, T.; Lakatos, M.; Bihari, Z.; Nagy, A.; Németh, A.; Kovacs, T.; Mihic, D.; Dacic, M.; et al. Climate of the Carpathian Region in 1961–2010: Climatologies and Trends of Ten Variables. *Int. J. Climatol.* **2014**, *35*, 1322–1341. [CrossRef]
64. Description of MASH and MISH Algorithms. Multiple Analysis of Series for Homogenization (MASH v3.03) by Szentimrey, T. p. 9–68, and Meteorological Interpolation Based on Surface Homogenized Data Basis (MISH v1.02) by Szentimrey, T.; Bihari, Z. p. 69–100. 2013. Available online: http://www.carpatclim-eu.org/docs/mashmish/mashmish.pdf (accessed on 6 April 2021).
65. Deliverable D2.10. Final Version of Metadata per Country of All National Gridded Datasets Created within Module 2. Annex 1—Metadata of the Daily Gridded Datasets per Country. 2013. Available online: http://www.carpatclim-eu.org/pages/deliverables/ (accessed on 6 April 2021).
66. Anomalies of Northern Hemisphere Annual Surface Air Temperature (MAAT) Since 1850 According to Hadley CRUT, a Cooperative Effort between the Hadley Centre for Climate Prediction and Research and the University of East Anglia's Climatic Research Unit (CRU). UK. Available online: https://crudata.uea.ac.uk/cru/data/temperature/HadCRUT5.0Analysis.pdf; https://crudata.uea.ac.uk/cru/data/temperature/#licence (accessed on 6 July 2021).
67. Péczely, G. *Climatology*; Tankönyvkiadó: Budapest, Hungary, 1974; p. 340. (In Hungarian)

68. Student's T-Test. Available online: https://stats.stackexchange.com/questions/344006/understanding-t-test-for-linear-regression (accessed on 29 March 2021).
69. Bartha, I. An objective decision procedure for prediction of maximum wind gusts associated with Cumulonimbus Clouds. *Idojaras* **1987**, *91*, 330–346.
70. Mika, J. Changes in weather and climate extremes: Phenomenology and empirical approaches. *Clim. Chang.* **2013**, *121*, 15–26. [CrossRef]